

1 A comprehensive investigation on afternoon transition of the atmospheric
2 boundary layer over a tropical rural site

3
4
5 A. Sandeep, T. Narayana Rao, and S. V. B. Rao#

6 *National Atmospheric Research Laboratory, Gadanki – 517 112, India*

7 *# Sri Venkateswara University, Department of Physics, Tirupati – 517 502, India*

8
9
10
11
12
13 Address for correspondence
14 Dr. T. Narayana Rao
15 Head, Clouds and Convective Systems Group
16 National Atmospheric Research Laboratory
17 Gadanki – 517 112, India
18 Mail: tnrao@narl.gov.in
19 Alt. Mail drtnr2001@yahoo.com
20 Phone: +91 8585 272 125
21

22
23
24
25
26
27 **Keywords:** Afternoon transition, Atmospheric boundary layer, Entrainment flux, sodar and wind
28 profilers.

1 **Abstract**

2 The transitory nature of the atmospheric boundary layer few hours before and after the time of
3 sunset has been studied comprehensively over a tropical station, Gadanki (13.45°N, 79.18°E),
4 using a suite of in situ and remote sensing devices. This study addresses the following
5 fundamental and important issues related to the afternoon transition (AT). Which state variable
6 first identifies it? Which variable best identifies it? Does the start time of AT varies with season
7 and height? If so, which physical mechanism is responsible for the observed height variation in
8 the start time of transition?

9 At the surface, the transition is first seen in temperature (T) and wind variance (σ^2_{ws}),
10 ~100 min prior to the time of sunset, then in vertical temperature gradient and finally in water
11 vapour mixing ratio variations. Aloft, both signal-to-noise ratio (SNR) and spectral width (σ)
12 show the AT nearly at the same time. The T at the surface and SNR aloft are found to be the best
13 indicators of transition. Their distributions for start time of AT with reference to time of sunset
14 are narrow and consistent in both total and seasonal plots. The start time of transition shows
15 some seasonal variation with delayed transitions occurring mostly in the rainy and humid season
16 of northeast monsoon. Interestingly, in contrast to the general perception, the signature of the
17 transition is first seen in the profiler data then in sodar data and finally in the surface data,
18 suggesting that the transition follows top-to-bottom evolution. It indicates that other forcings,
19 like entrainment, could also play a role in altering the structure of ABL during the AT, when the
20 sensible heat flux decreases progressively. These forcing terms are quantified using a unique
21 high-resolution dataset to understand their variation in light of the intriguing height dependency
22 of the start time of AT.

23

1 **1 Introduction**

2 The behaviour of atmospheric boundary layer (ABL) during the transition from well mixed layer
3 during the day to stably stratified layer during the night is quite complex and is also poorly
4 understood. In recent years, the afternoon transition (AT) and evening transition (ET) of the ABL
5 gained lot of attention for various reasons (Lothon et. al., 2014). These transitional regimes are
6 found to be important for the vertical transport of species, like pollutants, water vapour and
7 ozone (Klein et al., 2014), the inception and strength of the nocturnal low level jet (LLJ) (Mahrt,
8 1981; Van De Wiel et al., 2010), and the whole structure of the nocturnal boundary layer.
9 Further, identification of ABL becomes uncertain and there is no consensus on which scaling
10 laws (day-time convective scaling due to surface buoyancy flux? or nocturnal boundary layer
11 scaling due to surface wind stress?) would work well during this period (Pino et al., 2006).
12 Further, the start time of transition and its duration could be different at the surface and aloft,
13 because the turbulence may not immediately dissipate after the sunset (Busse and Knupp, 2012).

14 Researchers defined the transition in a variety of ways employing various parameters
15 obtained from different instruments. Some of them treated the transition as an instantaneous
16 process, while the others considered it as a process of few hours. The most popular and widely
17 used definition is the reversal of surface heat flux (positive to negative) (Grant, 1997; Acevedo
18 and Fitzjarrald, 2001; Beare et al., 2006; Angevine, 2008). A similar technique is employed by
19 Nieuwstadt and Brost (1986), in which the AT is assumed to occur following the cessation of
20 upward surface sensible heat flux. Edwards et al. (2006) noted that the shortwave heating starts
21 to decrease much before the surface heat flux changes its sign. They included the shortwave
22 heating in the definition of AT, which shifted the start of afternoon transition to an earlier time.
23 Acevedo and Fitzjarrald (2001) identified the start time of the transition from a sharp decrease in

1 the spatial temperature difference and end from the maximum spatial standard deviation of
2 temperature. As seen above, all these definitions are based on surface measurements and do not
3 account the physical processes occurring aloft during the transition.

4 The studies that used remote sensing measurements like wind profiling radars, sodars and
5 lidars focused more on the processes aloft (mostly in the lower part of ABL) to define the AT. In
6 a seminal study, Mahrt (1981) used a kinematic definition for AT period. According to Mahrt
7 (1981) the AT is a 4-5 h time period, starts from the time of low-level wind deceleration
8 (typically 2 h before the sunset) and ends when the flow at all levels turned towards the high
9 pressure. Grimsdell and Angevine (2002) and Angevine (2008), using radar wind profiler
10 measurements, noticed that both reflectivity (range-corrected signal-to-noise-ratio (SNR)) and
11 the spectral width (σ) (a measure of turbulence) decrease sharply during the AT. The
12 applicability of these approaches is always an issue, particularly when the turbulence is either
13 weak or strong throughout the day or when the turbulence increases due to some other processes
14 associated with katabatic winds or land sea-breeze circulations (Sastre et al., 2012). Instead of
15 defining the start and end times for AT, Busse and Knupp (2012) studied the variations in
16 meteorological parameters with reference to the sunset time. They noted an increase in wind
17 speed and a decrease in sodar return power in the lower ABL. They found that the AT has a
18 relatively consistent pattern regardless of season.

19 A few studies employed models to understand or validate the occurrence of different
20 types of transition (Brazel et al., 2005; Edwards et al., 2006; Pino et al., 2006; Sorbjan, 2007;
21 Nadeau et al., 2011; Sastre et al., 2012). Brazel et al. (2005) studied the evening transition under
22 weak synoptic forcing that favours the local thermal circulations and compared the observed
23 transitions with models. Recently, Sastre et al. (2012) identified 3 types of evening transitions

1 and evaluated performance of the Weather Research and Forecasting Advanced Research (WRF-
2 ARW) model in reproducing these transitions by varying PBL parameterization schemes. They
3 noted that all parameterizations reproduced the observed behaviour of AT in certain
4 circumstances. Noting the need to understand the transitions in a better way, several field
5 campaigns were conducted in recent years, employing both in situ and remote sensors,
6 exclusively for better characterisation and modelling of the transitions. For instance, Cooperative
7 Atmosphere-Surface Exchange Study (CASES-99) (Poulos et al., 2002), Boundary Layer Late
8 Afternoon and Sunset Turbulence (BLLAST) (<http://bllast.sedoo.fr/>)(Lothon et al., 2014) and
9 Phoenix Evening Transition Flow Experiment (TRANSFLEX) (Fernando et al., 2013).
10 Recently, manned and unmanned aerial vehicles were used to study the vertical structure of
11 lowest part of ABL during the AT (Bonin et al., 2013; Lothon et al., 2014).

12 Most of the above studies focussed on the variations in state variables, like temperature,
13 humidity, wind and turbulence, in the surface layer as they are easily accessible. Other studies
14 characterized the evening transitions aloft, but neglecting the variations at the surface. Only a
15 few studies that were based on campaign data and/or a few months of data dealt the transitions in
16 totality, i.e., studied the variations at the surface and aloft (Busse and Knupp, 2012; Fernando et
17 al., 2013; Lothon et al., 2014). Again, the data employed in those studies were limited, few days
18 to 2 months. Certainly there is a need to characterize and understand the transitions at the surface
19 and aloft in different seasons through systematic observations on a long-term basis. Further,
20 earlier studies used different state variables to define the transition. Only a few studies focused
21 on how these state variables vary with reference to the time of sunset (Busse and Knupp, 2012).
22 Although some tower-based observations exist in the literature, the complete understanding of
23 the transition over a deeper layer is certainly far from complete. This forms the basis for the

1 present study. In particular, the study tries to answer the following questions: how the surface
2 state variables and radar/sodar attributes vary during the transition and with reference to the time
3 of sunset? Which state variable better identifies the transition? How the start time of transition
4 varies with height and season? Which physical processes are responsible for the vertical
5 evolution of the transition?

6 The paper is organized as follows: Sect. 2. introduces the measurement site, data and
7 instrumentation employed. The variation of different state variables at the surface and aloft is
8 studied with the help of a typical case study in Sect. 3. The start time of AT as identified by
9 different state variables and their mean characteristics at the surface and aloft are studied with
10 reference to the time of sunset. The questions posed above are discussed in light of present
11 observations in Sect. 4. The important forcing terms on the ABL are estimated using a unique
12 dataset to understand the role of entrainment in the afternoon transition. The important results
13 are concluded in Sect. 5.

14

15 **2 Data and site description**

16 The present study follows an integrated approach, wherein several instruments available at
17 National Atmospheric Research Laboratory (NARL), Gadanki (13.45° N, 79.18° E) are
18 extensively used. This site is located ~ 375 m above the mean sea level in a rural area in southeast
19 peninsular India and is surrounded by hillocks (300-800 m within 10 km region) distributed in a
20 complex fashion. The rainfall in this region is influenced primarily by two monsoons, southwest
21 (June-September) and northeast (October-December) (Rao et al., 2009). Summer and winter are
22 the other two seasons, covering the months of March-May and January-February, respectively.

1 The present study relies on a variety of instruments, both in situ and remote sensors
2 (Table 1), whose measurements cover the entire ABL. Though these instruments provide several
3 other parameters, those used in the present study are only listed in Table 1. Two kinds of
4 datasets (we refer them here as dataset 1 and dataset 2) are used in the present study, but for
5 different purposes. Dataset 1 was collected with a suite of non-continuously operated
6 instruments, spanning a 3 year period. This dataset is being used to examine the seasonality and
7 height dependence of AT. It includes long-term observations made by an instrumented 15 m
8 tower (hereafter referred to as Mini Boundary Layer Mast – MBLM), a Doppler sodar and three
9 UHF wind profilers (operated at NARL, but during different years). Dataset 2 is comprised of
10 the intense observations, which include the instrumentation of dataset 1 along with a flux tower
11 having a sonic anemometer (RM Young 8100) at 8 m level and radiosondes (Meisei 90)
12 launched every three hours. Dataset 2 was collected over two, three day campaigns (one during
13 the monsoon and one during the winter). This dataset is being used to understand the role of
14 surface forcing and entrainment in triggering the AT.

15 The MBLM provides temperature (T), relative humidity (RH), wind speed (WS) and
16 wind direction (WD) data at 3 levels (5, 10 and 15 m) with 1 s temporal resolution. The type of
17 sensors used and their accuracies are given in Table 2. A Doppler sodar operating at a frequency
18 of 1.8 kHz and a peak power of 100 W provides the SNR, σ and wind information at 27 s and 30
19 m temporal and height resolutions, respectively (Anandan et al., 2008) (see Table 3 for more
20 details about different remote sensing instruments). The UHF wind profiler data consists of the
21 data from 3 wind profilers, operated during different years. An old UHF wind profiler (referred
22 to as Lower Atmospheric Wind Profiler - LAWP) was operated at a frequency of 1.375 GHz
23 during the period 1999-2000. Complete description of the system and specifications can be found

1 in Reddy et al. (2001) and Rao et al. (2001). It was operated in two modes; low mode covering
2 0.3 to 4.8 km and high mode covering 0.9 to 6.8 km, sequentially switching between each mode,
3 providing a temporal resolution of ~11 min. Recently, NARL has indigenously developed two
4 UHF wind profilers with the same frequency (1.28 GHz) but with different antenna dimensions
5 and transmitted powers. The smaller UHF wind profiler that uses an 8 x 8 antenna array covering
6 an area of 1.4 m x 1.4 m transmits a power of 0.8 kW (hereafter referred to as WPR_{8x8}).
7 Whereas, the larger profiler has a bigger antenna array of 2.8 m x 2.8 m with 16 x 16 elements
8 and high-transmitting power of 1.2 kW (hereafter referred to as WPR_{16x16}). Complete description
9 of these systems and their capabilities can be found in Srinivasulu et al. (2011, 2012). The
10 WPR_{8x8} was operated at NARL during May-September 2010, while the bigger WPR_{16x16} has
11 been in operation from October 2010. It can be seen from Tables 1 and 3 that these instruments
12 provide a unique long-term dataset from the surface to top of the ABL.

13 A series of automated tests were performed on tower time series data to identify
14 instrumentation problems, flux sampling problems, and physically plausible but unusual
15 situations (Burba, 2013). Further, clear-sky days are identified from shortwave radiation
16 measurements made by a pyranometer (Kipp and Zonen CMP6) located near the MBLM.
17 Omitting the days with large data gaps and rain/dense clouds, 423 days of surface data were
18 available for further analysis from 3 years of MBLM measurements. The range-time plots of
19 spectral moments (SNR, vertical velocity (w) and σ) from sodar and wind profiler are examined
20 for the clear growth and decay of ABL and convection/precipitation contamination (Grimsdell et
21 al., 2002; Rao et al., 2008). Based on the above criteria, a total of 530 and 482 clear-sky days of
22 sodar and profiler, respectively, were only selected (from dataset 1) for further analysis. To
23 examine whether the filtering of data for clear-sky days has caused any bias towards the dry

1 season (winter and summer), the data are segregated on the basis of season. Table 4 shows the
2 number of days for which the measurements were available, number of discarded days due to
3 rain/dense cloud or bad data quality and the number of days considered for the present study as a
4 function of season. Though considerable data were filtered out in the rainy seasons (southwest
5 and northeast monsoons), the number of available days is large enough to represent the season.
6 Also, the number of days available in the rainy season is of the same order as that of in other
7 seasons, indicating that the filtering has not biased the results towards any season.

8 Note that MBLM, sodar and wind profilers were operated during different years. Only 19
9 days of simultaneous clear-sky measurements (without large data gaps) from all the above
10 sensors were available. Measurements from these 19 days are used to understand the behavior of
11 AT at different altitudes. The total data (from different years, i.e., dataset 1) are used to obtain
12 robust statistics on the mean behavior of AT.

13

14 **3 Results and discussion**

15 **3.1 Typical evolution of AT from the surface to top of the ABL**

16 Figure 1 shows the diurnal variation of surface state variables (T , water vapour mixing ratio (r),
17 WS, wind variance (σ_{WS}^2) and wind direction (WD)) and sodar and profiler attributes (range-
18 corrected SNR (hereafter referred to simply as SNR), horizontal wind speed, σ , w and wind
19 direction) on 11 May 2010, providing a comprehensive paradigm of the typical evolution of
20 transitional boundary layer at the surface and aloft (up to 3.6 km). The surface state variables (at
21 5 m level) exhibit larger variations during the transition period than during rest of the night.
22 During the AT, as the shortwave heating decreases, the temperature decreases monotonically
23 (Fig. 1a) in clear-sky conditions, if temperature advection is neutral. Another signature of this

1 transition can be seen in short-term variability of surface parameters, highly variable during the
2 noon (associated with thermals) to smaller fluctuations in the night. The weakening of thermals
3 (both magnitude and their vertical extent) in the afternoon reduces the convective turbulence and
4 σ_{ws}^2 (Fig. 1d). This reduction weakens the downward transport of momentum and low-level
5 wind speed (Fig. 1c) (Mahrt, 1981; Acevedo and Fitzjarrald, 2001). The surface winds also
6 became less gusty during the transition. During the day, when the convective turbulence is
7 active, the low-level moisture gets diluted because of the transport of moisture by turbulence. As
8 the turbulence decreases during the transition, the low-level moisture having most of its sources
9 on the earth's surface increases in the absence of strong mixing (Fig. 1b). On some days, this
10 increase appears as a sudden jump, as also noted by earlier studies (Busse and Knupp, 2012), and
11 on the other days it is more gradual. The wind direction nearly remains the same from ~14 IST
12 (Indian Standard Time (IST) = UTC + 05:30) to mid-night (Fig. 1e).

13 To understand the transitions aloft, variation of sodar and profiler attributes are examined
14 in detail (Fig. 1f-o). Figure 1 clearly shows the transition of the ABL from a highly convective to
15 a more stable regime. When the convective turbulence is active during the day time, the thermals
16 are clearly apparent as columns of enhanced backscatter in the time-height SNR plot (Fig. 1k).
17 Though the thermals do not appear clearly in the SNR of sodar in this case, they appear very
18 clearly in other cases. These plumes are also visible in the w plot (Fig. 1i and n) as enhanced up-
19 and down-ward motions with w values exceeding $\pm 2 \text{ m s}^{-1}$ and as columns of enhanced
20 turbulence (Fig. 1g and l). The backscatter for sodar and profiler depends on the refractive index
21 irregularities caused primarily by turbulence-driven temperature and humidity variations. The
22 SNR is, therefore, high during the day, when the convectively-driven turbulence is active.
23 Nevertheless, about 2 h before the sunset, both the intensity and vertical extent of thermals start

1 to decrease continuously till the sunset occurs.. The minimum backscatter (SNR) is seen just
2 before the sunset, mainly due to the weak turbulence. The magnitude of backscatter and vertical
3 extent of sodar data again increase in accordance with the deepening of the inversion layer. As
4 noted by Busse and Knupp (2012), the winds within the nocturnal boundary layer generally
5 decrease during the AT, but increase above the nocturnal boundary layer. It makes the
6 identification of start time of AT using wind speed somewhat ambiguous. On the other hand, it
7 is rather easy to identify the start time of AT from the variations of SNR and σ . The wind
8 direction does not change much with altitude below 1.5 km and remains mostly easterly to
9 southeasterly (Fig. 1j and o). It doesn't change much with time also around the time of sunset
10 (few hours before and after the time of sunset), ruling out the possibility of advection of different
11 air masses causing the above changes.

12 When the surface heating reverses to cooling in the evening, both convection and
13 turbulence gradually reduces till the subsequent development of a stable boundary layer with
14 well-defined surface inversion layer. As a result, all state variables at the surface and aloft,
15 manifested primarily by the turbulence, vary considerably during this period. To better depict
16 this variability, MBLM- (T , r , σ^2_{WS} and ΔT (T_5-T_{10} , indicating the stability of the lower ABL, the
17 suffixes 5 and 10 indicate the height of temperature measurements in m)), sodar- and profiler-
18 derived state variables (SNR and σ at 3 representative levels; 150, 300 and 450 m for sodar and
19 900, 1500 and 2100 m for profiler) during the period 15:00–21:00 IST are plotted in Fig. 2. To
20 minimize random fluctuations and the chosen level more representative, the data are averaged
21 both in time (5 min for sodar and no temporal integration for profiler) and height (3 heights
22 centred on the chosen level). The time series surface data are then low-pass filtered using local
23 regression using weighted linear least squares and a 1st order polynomial model (using the

1 function 'lowess' in matlab). On 11 May 2010, the temperature (Fig. 2a) starts to decrease
2 monotonically, at the rate of 1-1.5 °C per 1 h, from 16:10 IST (dashed line), 152 min prior to the
3 time of sunset (solid vertical black line). Though the temperature decrement starts little early,
4 but is not consistent and also weak in magnitude. Another surface characteristic showing a
5 significant change during the AT is the mixing ratio (Fig. 2b), which clearly shows a gradual
6 increase from 16:10 IST. The temperature gradient (Fig. 2c) also reverses from positive to
7 negative few minutes after the 5 m level temperature starts to decrease. The wind variance (Fig.
8 2d), representing small-scale wind fluctuations and turbulence, also shows a decreasing trend
9 from 16:25 IST.

10 The sodar and profiler backscatter, depends primarily on turbulent irregularities of
11 refractive index, decreases with the waning of sensible heat flux (and thermals) during the
12 afternoon transition. On 11 May 2010, the SNR of sodar starts to decrease ~2 h 40 min prior to
13 the time of sunset at all heights. Interestingly, the start time of SNR reduction shows height
14 dependence with higher altitudes showing the reduction earlier. The SNR minimum is observed
15 10-20 min before the sunset at all heights, mainly due to the reduction in turbulent fluctuations in
16 temperature. Nevertheless, the SNR increases again after the sunset, following the formation of
17 an inversion layer. The σ (Fig. 2f) variations are quite similar to that of SNR during the
18 transition. The σ shows a decreasing trend 2 h 10-20 min prior to the sunset, whereas its
19 minimum is observed 10-30 min from the time of sunset. The profiler SNR and σ variations are
20 similar to that of sodar, except that their reduction starts little early. The profiler SNR and σ start
21 to decrease ~3 h prior to the time of sunset. Also, the SNR and σ minima are observed at around
22 the time of sunset. It is very interesting to note the height dependency in the time at which state

1 variables show large variation, i.e., it is seen first in profiler attributes then in sodar attributes and
2 finally in surface parameters.

3 **3.2 Distributions for start time of transition with reference to the time of sunset**

4 It is clear from the case study that surface parameters and sodar/profiler attributes show large
5 variations during the AT. The first and foremost problem, therefore, is to properly and
6 objectively identify the start time of AT from these state variables. It is also important to
7 recognize the state variable that unambiguously identifies the start time of transition. As seen in
8 case studies, state variables like T , ΔT , r and σ^2_{WS} at the surface and SNR and σ aloft can be used
9 for this purpose. For identifying the start time of AT, 19 days on which measurements of all
10 instruments (MBLM, sodar and profiler) are available are considered. The start time of AT is
11 identified manually from temporal variation of each state variable (like those shown in Fig. 2).
12 The temporal gradients are estimated for each state variable from all 19 cases, which are then
13 finally used to fix the thresholds. The start time of AT is identified from the variation of the each
14 state variable as follows.

15 Temperature: the time at which T starts to decrease by $\geq 0.5^\circ\text{C}$ in 30 min.

16 Water vapour mixing ratio: the time at which r increases by $\geq 0.5 \text{ g kg}^{-1}$ in 30 min.

17 Wind variance: the time at which σ^2_{WS} decreases by $\geq 0.1 \text{ m}^2 \text{ s}^{-2}$ in 30 min.

18 Temperature gradient: the time at which ΔT becomes positive to negative and remains negative
19 for at least an hour.

20 SNR: the time at which SNR decreases by $> 1 \text{ dB}$ in 30 min.

21 Spectral width: the time at which σ decreases by $\geq 0.1 \text{ m s}^{-1}$ in 30 min.

1 Note that all the above conditions should hold good for at least an hour from the start time of
2 transition. Also, all the above conditions are checked only in the data during 15:00-20:00 IST.

3 First, the average behaviour of the start time of AT, as identified by selected state
4 variables, with reference to the sunset (i.e., start time of AT – time of sunset) has been studied at
5 the surface and aloft. The distributions (from dataset 1) for start time of AT with reference to the
6 sunset (hereafter referred to as $\text{Trans}_{\text{sunset}}$ (start time of AT – time of sunset)) as obtained by
7 various state variables are shown in Fig. 3. These distributions are shown as box plots, where the
8 box comprises 50 % of values (25 and 75 percentile) and whiskers represent 5 and 95 percentile
9 values. On average, σ^2_{WS} and T show the first signature of AT among all surface state variables
10 (Fig. 3a), ~1 h 40 min prior to the time of sunset, followed by ΔT (1 h 18 min before sunset). The
11 last characteristic for transition is seen in r as a gradual increase (or jump) occurring, 1 h 10 min
12 prior to the time of sunset. The signature of transition can be seen as early (late) as 165 (45) min
13 before (after) the sunset in σ^2_{WS} (r) on some days. Except for temperature, all other surface state
14 variables show signature of transition even after the sunset. Though not many such cases are
15 found at Gadanki (can be seen from Fig. 3a), but late transitions are not uncommon, as they are
16 widely reported elsewhere (Acevedo and Fitzjarrald, 2001). The distribution of $\text{Trans}_{\text{sunset}}$ is
17 wider for r than for any other state variable, indicating that the jump in r occurs at different
18 timings with reference to the time of sunset. On the other hand, the start time of AT as obtained
19 by T is relatively consistent throughout the year, as evidenced by the narrow distribution (Fig.
20 3a).

21 Figure 3b-g shows distributions for $\text{Trans}_{\text{sunset}}$ as identified by selected sodar and profiler
22 attributes (SNR and σ) at 3 selected altitudes (150, 300 and 450 m for sodar and 900, 1500 and
23 2100 m for profiler). At any particular altitude, both SNR and σ shows the signature of transition

1 around the same time. Though small differences exist, they are not significant. Nevertheless, the
2 identification of transition start time is somewhat easy with SNR and is also consistent, as
3 evidenced by its relatively narrow distribution.

4 As seen in the case study, the mean start time of AT also shows height dependency and
5 follows top-to-bottom evolution, i.e., the signature of AT is seen first in the profiler data (~2 h 40
6 min before the time of sunset) then in sodar data (~2 h before the time of sunset) and finally in
7 MBLM measurements. Angevine (2008) also noted the deterioration of ABL structure aloft with
8 wind profiler preceding the start time of AT at the surface. It contradicts the general perception
9 that the entire ABL is controlled primarily by the underlying earth's surface and the start time of
10 transition should follow a bottom-up evolution. It is true that surface forcing is the defining
11 mechanism during the day, but it seems not the case during the transition, the time during which
12 other forces could also be important.

13 A sensitivity analysis is carried out to know the impact of the above chosen thresholds on
14 $\text{Trans}_{\text{sunset}}$ as obtained by different state variables. The chosen thresholds are varied by $\pm 20\%$ in
15 steps of 10% and the mean $\text{Trans}_{\text{sunset}}$ as obtained by different state variables is estimated at
16 different altitudes. The mean $\text{Trans}_{\text{sunset}}$ as a function of altitude is plotted in Fig. 4, which clearly
17 shows that the important results do not change much, even if we vary the thresholds by $\pm 20\%$.
18 For instance, the mean $\text{Trans}_{\text{sunset}}$ does not change much with the variation of thresholds. Also,
19 the height dependence of $\text{Trans}_{\text{sunset}}$ is strikingly apparent with all used thresholds. It suggests
20 that the observed variability in $\text{Trans}_{\text{sunset}}$, like top-to-bottom evolution, is not an artefact arising
21 due to the chosen thresholds. Regarding the usability of these thresholds at other sites, it appears
22 (from Fig. 4) that they possibly can be used at other tropical sites, which are in similar climatic
23 conditions as Gadanki region. Although we expect similar variations in most of the state

1 parameters at mid- and high-latitudes, the magnitude of variation could be different because of
2 the differences in the solar zenith angle and rate of reduction of solar radiation during the
3 transition. Therefore, some tuning of thresholds may be required at different latitudes.

4 **3.3 Seasonal variation in the start time of transition**

5 Since Gadanki experiences different seasonal patterns: very hot and dry summer, hot and rainy
6 southwest monsoon, cool and rainy northeast monsoon and cool and dry winter. These seasonal
7 factors (solar exposure, synoptic flow, soil condition, etc.) will have a different impact on ABL,
8 in general, transitions, in particular. Therefore, the distributions of $\text{Trans}_{\text{Sunset}}$ for different
9 seasons (Fig. 5) have been studied to understand the impact of the above factors on the start time
10 of transition. Figure 5a-d reveals that the order in which the surface state variables show the
11 transition remain nearly the same (monsoon season is an exception), but their occurrence time
12 with reference to the sunset varies considerably. Although reduced compared to the total data
13 (Fig. 3), the distribution, representing the variability within the season, of transition start time for
14 each state variable is quite wide. The $\text{Trans}_{\text{Sunset}}$ distribution for T shows a consistent pattern
15 regardless of season with small variability within the season and the transition starts 80-100 min
16 prior to the time of sunset. Nevertheless, it exhibits a clear seasonal variation with dry seasons
17 (winter and summer) showing the transition early (~110 min prior to the sunset time) compared
18 to rainy seasons (80 min prior to the sunset time). The distributions for other state variables also
19 show some seasonal variation with warm seasons showing the transition little earlier than cold
20 seasons. But their distributions are much wider than the observed weak seasonal variation.
21 Among all state variables, $\text{Trans}_{\text{Sunset}}$ distribution for r shows not only large seasonal variability
22 but also a wide distribution, indicating highly variable nature of r jump (i.e., starts at different
23 timings with reference to the sunset).

1 Two representative heights, 300 m from sodar and 1500 m from wind profiler, are chosen
2 to study the seasonal variation in transition start time aloft (Fig. 5e-1). Like in Fig. 3, there is not
3 much difference in the start time of transition by SNR and σ in any season and at any particular
4 altitude. Two observations are strikingly apparent from Fig. 5. 1. Both profiler- and sodar-
5 derived start time of transition shows some seasonal variation with delayed transition during the
6 northeast monsoon, consistent with the seasonal variation at the surface. 2. Irrespective of the
7 season, the height dependency in transition start time is intact. Both these issues are discussed in
8 detail in Sect. 4.

9

10 **4 Discussion**

11 The four major questions related to the start time of transition that the paper tries to answer are,
12 (i) which state variable better identifies it, (ii) does it exhibits any seasonal variation (iii) does it
13 shows any height dependency?, and (iv) which physical mechanism is responsible for the
14 observed height variation of $\text{Trans}_{\text{sunset}}$?

15 (i) Among all state variables, the decrease of temperature at the surface and SNR aloft are
16 strikingly apparent in all case studies, which makes them ideal to identify the start time of AT.
17 Further, the distributions of $\text{Trans}_{\text{sunset}}$ for T and SNR are somewhat consistent and narrower than
18 that for other state variables. Although several earlier studies employed reversal of sign in
19 surface heat flux as a criterion for transition (Lothon et al., 2014 and references therein), it is
20 now well known that such a reversal not always occurs during the transition (Busse and Knupp,
21 2012). The formation of an inversion depends on several other factors and therefore the
22 formation of inversion alone cannot be used to define the transition. A few studies used
23 deceleration of low-level wind as a criterion for identifying the transition (Mahrt, 1981). The

1 above criterion works well in the lower portion of ABL, but fails above the nocturnal boundary
2 layer, where the wind accelerates in the frictionless fluid. Therefore, T at the surface and SNR
3 aloft can be used to identify the start time of transition, as also suggested by Edwards et al.
4 (2006).

5 (ii) The start time of transition as defined by different state variables shows some seasonal
6 variation, with late transitions during the northeast monsoon season. Though Gadanki receives
7 55% of the annual rainfall in the southwest monsoon, rising instantaneous soil moisture levels,
8 but the high insolation and temperatures immediately consume the soil moisture for latent
9 heating. On the other hand, this region also gets good amount of rainfall during the cool
10 northeast monsoon (Rao et al., 2009). The soil moisture levels, therefore, remain high in this
11 season. It is known from earlier studies that the abundance of soil moisture not only produces
12 shallow ABL but also delays the growth of the ABL (Sandeep et al., 2014). It appears from
13 present observations that not only the growth but also the descend (or transition) is getting
14 delayed due to the excess soil moisture.

15 (iii) The total and seasonal distributions of $\text{Trans}_{\text{sunset}}$ for different state variables at the surface
16 and aloft clearly show the height dependency in the start time of transition, following a top-to-
17 bottom evolution. It is known from the literature that there exists an apparent contradiction
18 between those who think the transition starts in the afternoon at high levels (Angevine, 2008) and
19 others who believe the AT occurs around the sunset and follows a bottom-up evolution. The
20 present study supports the former view, as similar evolution is seen in total and seasonal plots
21 (Figs. 3 and 5). During the AT, when the surface buoyancy flux decreases toward zero, the
22 influence of other competing processes like advection, and entrainment becomes relatively more
23 important (Bosveld et al., 2014). Therefore an attempt has been made to estimate these fluxes

1 (buoyancy and entrainment) to understand their roles in the observed height dependency in
 2 transition start time.

3 The ratio between the vertical kinematic eddy heat flux at the top of ABL and kinematic
 4 eddy heat flux at the surface (entrainment ratio) (Sun et al., 2008), as given below, therefore,
 5 becomes a fundamental and decisive parameter.

$$6 \quad A_R = -\frac{\overline{(w|\theta|)}_{zi}}{\overline{(w|\theta|)}_s} \quad \dots (1)$$

7 The heat flux at the top of ABL (or entrainment flux) is estimated following Angevine (1999).
 8 The entrainment can occur due to any or all of these factors, (1) when there is a shift in the ABL
 9 height (2) due to wind shear at the surface, (3) due to wind shear at the top of the ABL and (4)
 10 advection.

$$11 \quad -\overline{(w|\theta|)}_{zi} = A_0 + (A_2 u_*^2 u + A_3 \Delta u_h^3) \cdot (\theta_{vo}/g d_l) + (U \frac{\partial T}{\partial x} + V \frac{\partial T}{\partial y}) \quad \dots (2)$$

12 where u_* is the friction velocity, u the surface horizontal velocity (8 m in our case), Δu_h the wind
 13 shear at the top of ABL, g the acceleration due to gravity, θ_{vo} the virtual potential temperature at
 14 the surface, d_l is the depth of entrainment zone and A_2 and A_3 are empirical constants, $A_2=0.005$
 15 and $A_3=0.01$ (Stull, 1976). For the estimation of advection (last term in Eq. 2), the temperature
 16 (T), horizontal distance in zonal and meridional planes (∂x and ∂y , respectively, and is equal to
 17 0.5°) and zonal (U) and meridional (V) wind velocities near the top of ABL are taken from
 18 ECMWF Interim Reanalysis data (Dee et al., 2011). A_0 is the entrainment flux in the absence of
 19 any mechanical term contribution and is expressed as $w_e \Delta \theta$, w_e is the entrainment velocity and is
 20 estimated as follows.

$$21 \quad w_e = \frac{dz_i}{dt} - \bar{w} \quad \dots (3)$$

1 where \bar{w} is the average vertical velocity at the top of ABL and $\Delta\theta$ the vertical gradient in θ_v at
2 the top of ABL. As seen above, the time and space scales of different entrainment processes
3 cover a wide range, which makes it difficult to measure or model accurately (Angevine 1999).
4 Although it is possible to quantify the entrainment flux from heat budget equation (Eq. 2), the
5 uncertainties in the basic parameters (for instance, those in the advection term and w) hamper the
6 accuracy of the flux. Therefore, as also pointed by Angevine (1999), these numbers need to be
7 considered as ‘best available estimates’.

8 It is clear from above equations that profiles of meteorological parameters such as T ,
9 RH/r and w are essential to estimate the entrainment ratio. Though w can be obtained
10 continuously from the wind profiler, continuous measurement of T and RH/r at the top of ABL is
11 a difficult task. We, therefore, considered two 3 days campaign data (one each from southwest
12 monsoon and winter), wherein radiosonde ascents were made once in ~ 3 h, for a detailed study
13 (dataset 2).

14 Figure 6a-c shows the time-height variation of SNR, w and σ on 22 July 2011, depicting
15 the typical diurnal evolution of ABL during the campaign period. The θ_v profiles during
16 morning-evening (at 08:24, 11:54, 14:25 and 17:15 IST) period are shown in Fig. 6d to depict
17 the height of ABL (and also the gradients in θ_v at the top of the ABL). Clearly, the height of
18 ABL as obtained by the profiler (shown with dots on SNR plot) and radiosonde (the gradient in
19 θ_v profile) corresponds well. The agreement between them is also good in the diurnal variation,
20 with both the measurements showing shallow ABL in the morning and evening transition periods
21 and deep ABL during the day, when the ABL is convectively active.

22 The start time of AT as seen by different state variables at the surface and aloft on all
23 days during the two campaigns is shown in Fig. 7a and b. It clearly reiterates the height

1 dependency of start time of AT seen in Figs. 2-5, i.e., the start time of AT observed by profiler
2 precedes surface state variables on all days and in both seasons. Though the same pattern is seen
3 on all days, but the time at which the transition starts varies considerably from day to day.

4 The entrainment flux at the top of ABL is estimated by combining the measurements of
5 radiosonde ($\Delta\theta$, d_I), profiler (w , Δu_n), MBLM (u , θ_{vo}) and a meteorological flux tower (u_*) with
6 ECMWF interim data (advection term). The sensible heat flux and u_* at the surface required to
7 quantify the entrainment ratio (Eq. 1) are estimated following the eddy covariance method by
8 using 20 Hz resolution ultrasonic anemometer measurements at 8 m level. These fluxes are
9 evaluated at 30 min resolution.

10 Figures 8a and b shows the sensible and entrainment fluxes at ~ 3 h resolution during the
11 day, depicting the forcing on the ABL from bottom and top. The sensible heat flux varies
12 considerably during the day, with fluxes varying from 0.15 - 0.25 K ms^{-1} around noon ($\sim 11:00$
13 and $\sim 14:00$ IST) to 0.02 - 0.07 K ms^{-1} during the morning and evening transitions ($\sim 08:00$ and
14 $\sim 17:00$ IST). On the other hand, the entrainment flux neither changes drastically during the day
15 nor shows a clear diurnal cycle (compared to sensible heat flux). The magnitude of entrainment
16 flux depends mostly on the first term in Eq. 2, while the shear (2 and 3 terms in Eq. 2)
17 contributes very little to the total entrainment flux (not shown). Since the buoyancy flux changes
18 considerably, the entrainment ratio varies significantly during the course of the day. The
19 entrainment ratio increases to 0.5 - 1.1 during the morning and evening transitions. Therefore, it is
20 very clear from these observations that the forcing from the top (i.e., entrainment flux) becomes
21 very important, when the buoyancy flux is weak (i.e., during the transitions and night) A few
22 earlier studies also underscored the importance of buoyancy flux in altering the structure of
23 ABL. The entrainment not only modifies the top of the ABL but also impacts the entire depth of

1 the ABL (Lohou et al., 2010). Caughey and Kaimal (1977), have shown experimentally that the
2 heat flux descends suddenly during the transition, approximately an hour before the sunset, and
3 the reversal of heat flux (from positive to negative) first occurs at higher altitudes and then
4 propagates downwards to the surface, indicating the importance of entrainment heat flux in the
5 top-to-bottom evolution of the transition. Also, with continuous waning of sensible heat flux
6 during the AT, both the vertical extent and strength of thermals (can be seen in Figs. 1 and 6)
7 decrease monotonously. At the same time, the surface forcing (heating) remains good enough to
8 maintain the turbulence close to the surface and therefore does not show the signature of
9 transition, but delays it at the surface (Angevine, 2008).

10

11 **5 Conclusions**

12 This study presents a comprehensive view on the AT in terms of understanding the variability of
13 different state variables using a suite of in-situ and remote sensing measurements at Gadanki.
14 The study aims to address the following issues related to the start time of AT with a unique and
15 statistically robust data set (~3 years). Which parameter first shows the signature of transition at
16 the surface and aloft? Which parameter better defines or identifies it? How does it varies with
17 altitude and season? Which physical mechanism explains the observed vertical variation of
18 transition?

19 (i) Among the surface state variables, the signature of transition is first seen in σ_{ws}^2 and T data,
20 both of which start decreasing monotonically ~100 min prior to the time of sunset. The r
21 increase is the last signature of transition, while the reversal of ΔT variation from positive to
22 negative falls in between these extremes. Aloft, both SNR and σ identify the start of AT at the
23 same time, 120-160 min prior to the time of sunset, depending on the height considered. The

1 observed mean start time of AT (2 h prior to the sunset), obtained from SNR and σ variations,
2 matches well with that obtained by Mahrt (1981), who used horizontal wind reduction for
3 identifying the transition.

4 (ii) At the surface, the start time of AT can be discerned more easily from variations of T than
5 from that of σ_{ws}^2 , r and ΔT . While σ_{ws}^2 and ΔT variations show large modulations with time, r
6 variation is ambiguous at times. Also, the temperature reduction is more consistent with
7 relatively narrow distribution and occurs always before the sunset. Aloft, SNR variation is
8 robust in identifying the transition compared to ambiguous variations in horizontal wind velocity
9 (decreases at lower altitudes and increases at higher altitudes).

10 (iii) The start time of AT as defined by different state variables show some seasonal variation,
11 with delayed transitions during the northeast monsoon at the surface and aloft. Though there is
12 some seasonal variation in the start time of AT relative to sunset time, the order in which the
13 signature of AT is seen in different state variables (first in T , and σ_{ws}^2 followed by ΔT and r)
14 remained nearly the same in all seasons.

15 (iv) Interestingly, the start time of AT exhibits a clear height dependency, i.e., the signature of
16 transition is seen first in profiler attributes (~160 min) followed by sodar attributes (~120 min)
17 and finally in surface state variables (~100 min), suggesting that the transition follows a top-to-
18 bottom evolution (Angevine, 2008). The fact that the first signatures of transition are seen at
19 higher altitudes by profiler/sodars than at the surface suggests that the forces other than the
20 buoyancy could also play an important role during the transition. With continuous waning of
21 sensible heat flux (and surface forcing) during the AT, both the vertical extent and strength of
22 thermals decrease steadily (as seen in Figs. 1 and 6), triggering the descend of ABL or transition.
23 However, the surface heating is good enough to maintain the state variables and delay the

1 decrease of T and σ_{ws}^2 (considered to be the signatures of transition). Further, the impact of
2 forcings from top and bottom on the ABL is studied by quantifying the sensible and entrainment
3 fluxes, using a flux tower and profiler-radiosonde measurements, respectively. Though the
4 sensible heat flux varied significantly during the day, the entrainment flux remained nearly the
5 same throughout the day. The entrainment ratio increases considerably during the morning and
6 evening transitional periods, primarily due to the weak sensible heat flux. Therefore, the
7 entrainment flux appears to be playing a major role during the transition period (and in the night)
8 during which the sensible heat flux continuously weakens.

9

10 *Acknowledgements.* The authors would like to thank M. Venkat Ratnam for providing the GPS
11 radiosonde used in the present study (experiments are conducted under the special campaign of
12 Tropical Tropopause Dynamics (TTD) as a part of CAWSES-Phase II programme, India).

13

14

15

16

17

18

19

20

21

22

23

24

25

26

27

1 **References**

- 2 Acevedo, O. C., and Fitzjarrald, D. R.: The early evening surface-layer transition: Temporal and
3 spatial variability, *J. Atmos. Sci.*, 11, 2650–2667, 2001.
- 4 Anandan, V. K., Shrivankumar, M., and Srinivasarao, I.: First results of experimental tests of
5 newly developed NARL phased array Doppler sodar, *J. Atmos. Ocean. Tech.*, 25, 1778-
6 1784, 2008.
- 7 Angevine, W. M.: Entrainment results including advection and case studies from the Flatland
8 boundary layer experiments, *J. Geophys. Res.*, 104, 30947-30963, 1999.
- 9 Angevine, W. M.: Transitional, entraining, cloudy, and coastal boundary layers, *Acta Geophys.*,
10 56, 2–20, 2008.
- 11 Beare, R. J., Edwards, J. M., and Lapworth, A. J.: Simulation of the observed evening transition
12 and nocturnal boundary layers: Large-eddy modelling, *Q. J. R. Meteor. Soc.*, 132, 61–80,
13 2006.
- 14 Bonin, T., Phillip, C., Brett, Z., and Fedorovich, E.: Observations of the early evening boundary-
15 layer transition using a small unmanned aerial system, *Bound. -Lay. Meteorol.*, 146, 119–
16 132, 2013.
- 17 Bosveld, F. C., Baas, P., Steeneveld, G. J., Holtslag, A. A. M., Angevine, W. M., Bazile, E.,
18 Bruijn, E. I. F. D., Deacu, D., Edwards, J. M., Michael, E. K., Larson, V. E., Pleim, J. E.,
19 Raschendorfer, M., and Svensson, G.: The third GABLS intercomparison case for
20 evaluation studies of boundary-layer models. Part B: Results and process understanding,
21 *Bound. -Lay. Meteorol.*, 152, 157-187, doi:10.1007/s10546-014-9919-1, 2014.
- 22 Brazel, A. J., Fernando, H. J. S., Hunt, J. C. R., Selvor, N., Hedquist, B. C., and Pardyjak, E.:
23 Evening transition observations in Phoenix, Arizona, *J. Appl. Meteorol.*, 44,99-112,
24 2005.

1 Burba, G.: Eddy covariance method for scientific, industrial, agricultural, and regulatory
2 applications, LI-COR Biosciences, Nebraska, 331pp., 2013.

3 Busse, J., and Knupp, K.: Observed characteristics of the afternoon-evening boundary layer
4 transition based on sodar and surface data, *J. Appl. Meteorol. Climatol.*, 51,571-582,
5 2012.

6 Caughey, S., and Kaimal, J.: Vertical heat flux in the convective boundary layer, *Q. J. Roy.
7 Meteor. Soc.*, 103, 811-815, 1977.

8 Dee, D. P., Uppala, S. M., Simmons, A. J., Berrisford, P., Poli, P., Kobayashi, S., Andrea, U.,
9 Balmaseda, M. A., Balsamo, G., Bauer, P., Bechtold, P., Beljaar, A. C., van de Berg, L.,
10 Bidlot, J., Bormann, N., Delsol, C., Dragani, R., Fuentes, M., Geer, A.J., Haimberger, L.,
11 Healy, S. B., Hersbach, H., Hólm, E.V., Isaksen, L., Kållberg, P., Höhler, M., Matricardi,
12 M., McNally, A. P., Monge-Sanz, M., Morcrette, J.-J., Park, B.-K., Peubey, C., de
13 Rosnay, P., Tavolato, C., Thépaut, J.-N., and Vitart, F.: The ERA-Interim reanalysis:
14 configuration and performance of the data assimilation system, *Q. J. Roy. Meteor. Soc.*,
15 137, 553-597, 2011.

16 Edwards, J. M., Beare, R. J., and Lapworth, A. J.: Simulation of the observed evening transition
17 and nocturnal boundary layers: Single-column modelling, *Q. J. Roy. Meteor. Soc.*, 132,
18 61–80, 2006.

19 Fernando, H. J. S., Verhoef, B., Sabatino, S. Di., Leo, L. S., and Park, S.: The Phoenix evening
20 transition flow experiment (TRANSFLEX), *Bound. -Lay. Meteorol.*, 147, 443-468, doi:
21 10.1007/s10546-012-9795-5, 2013.

22 Grant, A. L. M.: An observational study of the evening transition boundary-layer, *Q. J. Roy.
23 Meteor. Soc.*, 123, 657–677, 1997.

1 Grimsdell, A.W., and Angevine, W.M.: Observations of the afternoon transition of the
2 convective boundary layer, *J. Appl. Meteor.*, 41, 3–11, 2002.

3 Klein, P. M., Hu, X. M., and Xue, M.: Impacts of mixing processes in nocturnal atmospheric
4 boundary layer on urban ozone concentrations, *Bound. -Lay. Meteorol.*, 150, 107-130,
5 doi: 10.1007/s10546-013-9864-4, 2014.

6 Lohou, F., Said, F., Lohou, M., Durand, P., and Serça, D.: Impact of boundary layer processes
7 on near-surface turbulence within the West Africa monsoon, *Bound. -Lay. Meteorol.*,
8 136, 1-23, 2010.

9 Lohou, M., Lohou, F., Pino, D., Couvreur, F., Pardyjak, E. R., Reuder, J., Vilà-Guerau de
10 Arellano, J., Durand, P., Hartogensis, O., Legain, D., Augustin, P., Gioli, B., Lenschow,
11 D. H., Faloon, I., Yague, C., Alexander, D. C., Angevine, W. M., Bargain, E., Barrié, J.,
12 Bazile, E., Bezombes, Y., Blay-Carreras, E., van de Boer, A., Boichard, J. L., Bourdon,
13 A., Butet, A., Campistron, B., de Coster, O., Cuxart, J., Dabas, A., Darbieu, C., Deboudt,
14 K., Delbarre, H., Derrien, S., Flament, P., Fourmentin, M., Garai, A., Gibert, F., Graf, A.,
15 Groebner, J., Guichard, F., Jiménez, M. A., Jonassen, M., van den Kroonenberg, A.,
16 Magliulo, V., Martin, S., Martinez, D., Mastrorillo, L., Moene, A. F., Molinos, F.,
17 Moulin, E., Pietersen, H. P., Pignatelli, B., Pique, E., Román-Cascón, C., Rufin-Soler, C.,
18 Saïd, F., Sastre-Marugán, M., Seity, Y., Steeneveld, G. J., Toscano, P., Traullé, O.,
19 Tzanos, D., Wacker, S., Wildmann, N., and Zaldei, A.: The BLLAST field experiment:
20 Boundary-Layer Late Afternoon and Sunset Turbulence, *Atmos. Chem. Phys.*, 14,
21 10931–10960, doi:10.5194/acp-14-10931-2014, 2014.

22 Mahrt, L.: The early evening boundary layer transition, *Q. J. Roy. Meteor. Soc.*, 107, 329-343,
23 1981.

- 1 Nadaeau, D. F., Pardyjak, E. R., and Higgins, C. W.: A simple model for the afternoon and early
2 decay of convective turbulence over different land surfaces, *Bound. -Lay. Meteorol.*, 141,
3 301-324, 2011.
- 4 Nieuwstadt, F. T. M., and Brost, R. A.: The decay of convective turbulence, *J. Atmos. Sci.*, 43, ,
5 532-546, 1986.
- 6 Pino, D., Jonker, H. J. J., Arellano, J. V. G., and Dosio, A.: Role of shear and the inversion
7 strength during sunset turbulence over land: characteristic length scales, *Bound. -Lay.*
8 *Meteorol.*, 121, 537-556, doi:10.1007/s10546-006-9080-6, 2006.
- 9 Poulos, S. G., Blumen, W., Fritts, D. C., Lundquist, J. K., Sun, J., Burns, S. P., Nappo, C., Banta,
10 R., Newsom, R., Cuxart, J., Terradellas, E., Balsley, B., and Jensen, M.: A
11 comprehensive investigation of the stable nocturnal boundary layer, *B. Am. Meteorol.*
12 *Soc.*, 83, 555–581, 2002.
- 13 Rao, T. N., Rao, D. N., and Mohan, K.: Classification of tropical precipitating systems and
14 associated Z–R relationships, *J. Geophys. Res.*, 116, 17699–17711, 2001.
- 15 Rao, T. N., Kirankumar, N.V.P., Radhakrishna, B., Rao, D. N., and Nakamura, K.: Classification
16 of tropical precipitating systems using wind profiler spectral moments part I: algorithm
17 description and validation, *J. Atmos. Ocean. Tech.*, 25, 884–897,
18 doi:10.1175/2007JTECHA1031.1, 2008.
- 19 Rao, T. N., Radhakrishna, B., Nakamura, K., and Prabhakara Rao, N.: Differences in raindrop
20 size distribution from southwest monsoon to northeast monsoon at Gadanki, *Q. J. Roy.*
21 *Meteorol. Soc.*, 135, 1630-1637, 2009.

1 Reddy, K. K., Kozu, T., Nakamura, K., Ohno, Y., Srinivasulu, P., Anandan, V. K., Jain, A. R.,
2 Rao, P. B., Rao, R. R., Vishwanathan, G., Rao, D. N.: Lower atmospheric wind profiler at
3 Gadanki, tropical India: Initial results, *Meteorol. Z.*, 10, 457-466, 2001.

4 Sandeep, A., Rao, T. N., Ramkiran, C. N., and Rao, S. V. B.: Differences in atmospheric
5 boundary-layer characteristics between wet and dry episodes of the Indian summer
6 monsoon, *Bound. -Lay. Meteorol.*, 153, 217-236, doi: 10.1007/s10546-014-9945-z, 2014.

7 Sastre, M., Yague, C., Roman, C. C., Maqueda, G., Salamanca, F., and Viana, S.: Evening
8 transitions of the atmospheric boundary layers: characterization case studies and WRF
9 simulations, *Adv. Sci. Res.*, 8, 39-44, 2012.

10 Sorbjan, Z.: A numerical study of daily transitions in the convective boundary layer, *Bound. -*
11 *Lay. Meteorol.*, 123, 365-383, doi: 10.1007/s10546-006-9147-4, 2007.

12 Srinivasulu, P., Yasodha, P., Kamaraj, P., Jayaraman, A., Reddy, S. N., and Satyanarayana, S.:
13 Simplified active array L-band radar for atmospheric wind profiling: initial results, *J.*
14 *Atmos. Ocean. Tech.*, 28, 1436-1447, doi: 10.1175/JTECH-D-11-00011.1, 2011.

15 Srinivasulu, P., Yasodha, P., Kamaraj, P., Rao, T. N., Jayaraman, A., Reddy, S. N., and
16 Satyanarayana, S.: 1280-MHz active array radar wind profiler for lower atmosphere:
17 System description and data validation, *J. Atmos. Ocean. Tech.*, 29, 1455-1470,
18 doi:10.1175/JTECH-D-12-00030.1, 2012.

19 Stull, R.B.: The energetics of entrainment across a density interface, *J. Atmos. Sci.*, 33, 1260-
20 1267, 1976.

21 Sun, J., and Wang, Y.: Effect of the Entrainment Flux Ratio on the Relationship between
22 Entrainment Rate and Convective Richardson Number, *Bound. -Lay. Meteorol.*, 126,
23 237-247, doi:10.1007/s10546-007-9231-4, 2008.

1 Van de Wiel, B. J. H., Moene, A. F., Steenveld, G. J., Baas, P., Bosveld, F. C., and Holtslag, A.
2 A. M.: A conceptual view on inertial oscillations and nocturnal low-level jets, *J. Atmos.*
3 *Sci.*, 67, 2679-2689, doi: 10.1175/2010JAS3289.1, 2010.

4

5

6

7

8

9

10

11

12

13

14

15

16

17

18

19

20

21 **Table 1.** Instruments used in the integrated approach, their operating frequency, height coverage, vertical and temporal resolutions and
 22 duration of data.

Instrument	Frequency of operation	Measured parameters	Height coverage	Vertical resolution	Temporal resolution	Period used
SODAR	1.8 kHz	SNR, winds and σ	0.03 - 1.5 km	30 m	27 sec	2007-2010
LAWP	1.357 GHz	SNR, winds and σ	0.3 - 4.2 km	150 m	~11 min	1999-2000
WPR _{8x8}	1.280 GHz	SNR, winds and σ	0.3 - 6.15 km	150 m	~10 min	2010
WPR _{16x16}	1.280 GHz	SNR, winds and σ	0.75 - 5.025 km	75 m	~10 min	2010-2011
MBLM		T , r , pressure, WS, WD and short wave radiation	5 - 15 m	5 m	1 s	2009-2011
GPS Radiosonde		T , RH, pressure	0 - 30 km	100 m	3 h	17-19 January 2011 21-24 July 2011
50 m Tower		Sonic temperature, vertical wind	8 m		0.05 s	17-19 January 2011 21-24 July 2011

23

24

25

26

27

28

29 **Table 2.** Details of measured parameters and sensors (make, model number, resolution and accuracy) on MBLM.

Parameter	Make	Model No.	Resolution	Measurement height	Accuracy
Wind Speed and Wind Direction	RM Young	05103V	1 Hz	5, 10 and 15m	0.3 m s ⁻¹ and 2°
Temperature and Relative Humidity	Rotronics	Hygroclip S3	1 Hz	5, 10 and 15m	0.3° C and 2%
Pressure	Komoline	KDS-021	1 Hz	1.2 m	1hPa
Short Wave Radiation	Kipp & Zonen	CMP 6	1 Hz	1.2 m	1 W m ⁻²

40

41

42

43

44

45

46

47

48

49

50

51

52

53

54

55

56 **Table 3.** Major specifications of SODAR, LAWP, WPR_{8x8} and WPR_{16x16}

Parameter	SODAR	LAWP	WPR _{16x16}	WPR _{8x8}
Operating frequency	1.8 kHz	1357.5 MHz	1280 MHz	1280 MHz
Peak power	100 W	1 kW	1.2 kW	0.8 kW
Antenna array	1 m x 1 m	3.8 m x 3.8 m	2.8 m x 2.8 m	1.4 m x 1.4 m
Pulse width	180 ms	1 μ s (uncoded)	4 μ s (coded)	1 μ s (uncoded)
Inter pulse period (μ s)	9x10 ⁶	40	55	55
No. of Coherent Integrations	1	70	64	32
No. of Incoherent Integrations	1	100	20	20
No. of FFT points	4096	128	1024	1024
Beam width (deg)	4	3	5	6.5
Range resolution (m)	30	150	75	150
Beam directions*	N16, Z, E16	E15, Z, N15	E15, W15, Z, N15, S15	E10N10, W10S10, Z, W10N10, E10S10

* E, W, Z, N and S denote east, west, zenith, north and south directions, respectively, and the number indicates the off-zenith angle.

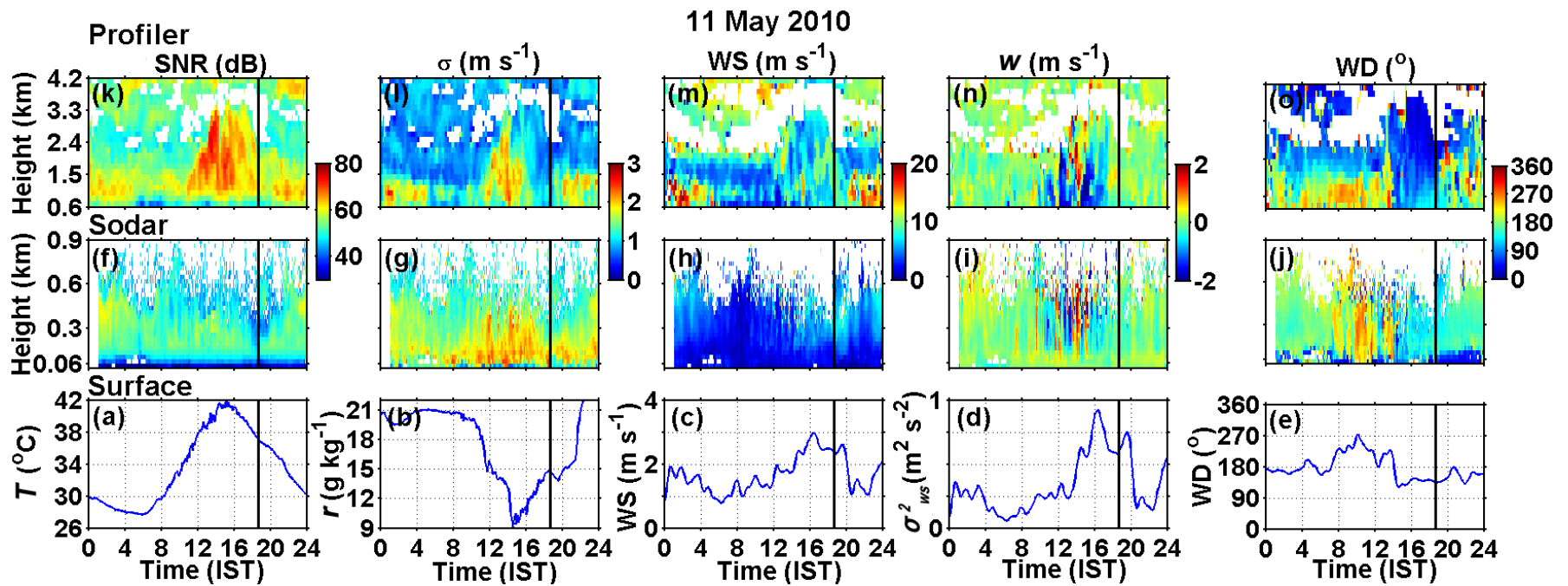
57
58
59
60
61
62
63

1
2
3
4
5

Table 4: Details of dataset 1 grouped as a function of season, showing the total number of days for which data are available, number of discarded days due to cloudy sky/rain or data gaps and number of clear days finally used in the present study. Win, Sum, SWM and NEM stand for, respectively, winter, summer, southwest monsoon and northeast monsoon.

Season	15m Tower (2009-2011)				Sodar (2007-2010)				Profiler (1999-00, 2010-11)			
	Win	Sum	SWM	NEM	Win	Sum	SWM	NEM	Win	Sum	SWM	NEM
Total no. of days	113	195	263	221	207	333	414	255	108	238	381	264
Discarded days	25	55	158	130	105	152	282	189	41	101	227	140
Clear days	88	140	105	91	102	181	132	66	67	137	154	124

6
7
8
9
10
11

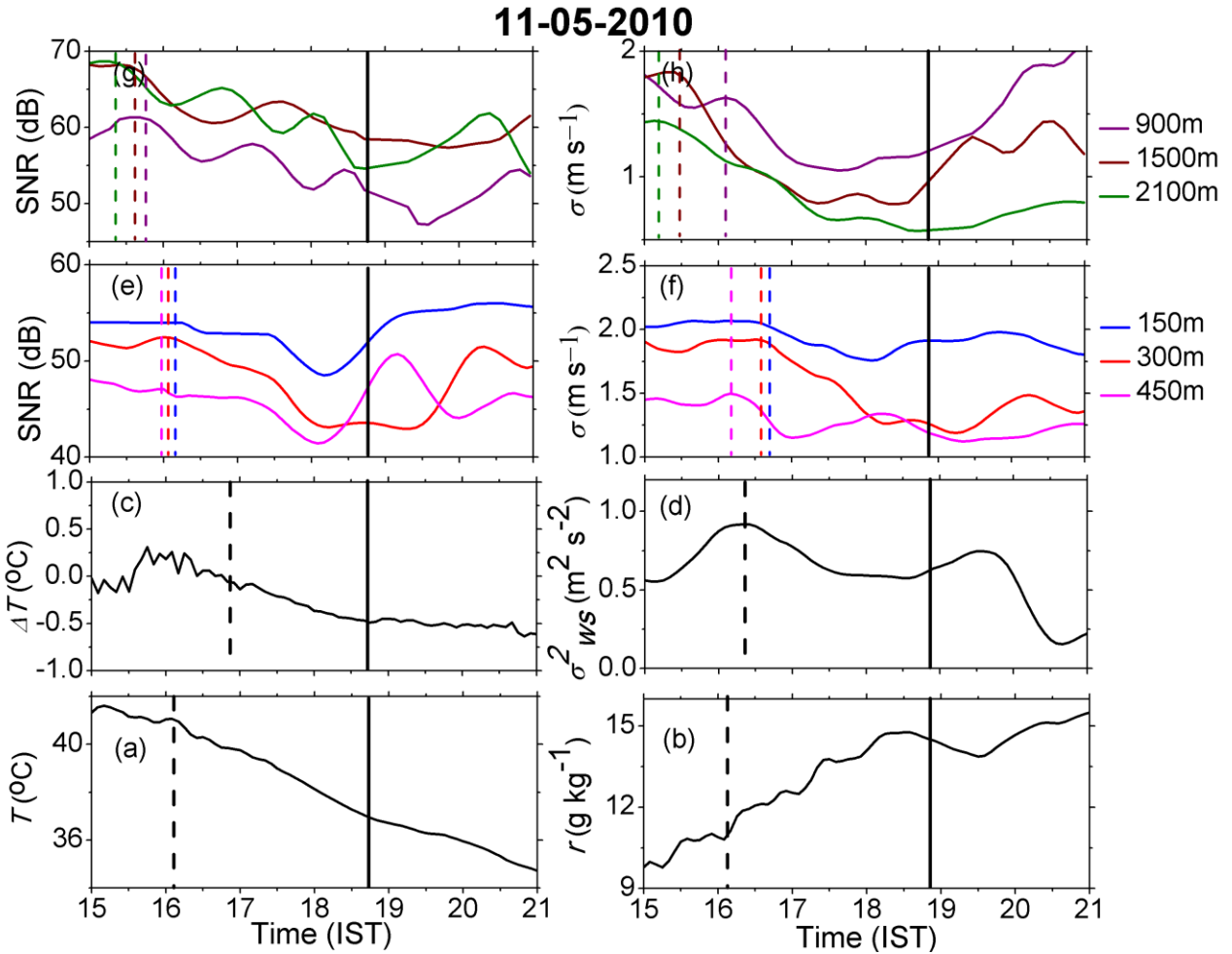


1

2 Figure 1: Diurnal variation of state variables at the surface and aloft on 11 May 2010, MBLM-derived surface (a) T , (b) r , (c) WS (d)
 3 σ_{ws}^2 and (e) WD and sodar-derived (f) range-corrected SNR, (g) σ , (h) WS, (i) w and (j) WD. (k-o) same as (f-j), except for profiler-
 4 derived state variables. The solid vertical line indicates the time of sunset.

5

1



2

3

4 Figure 2: Temporal variation of state variables (at the surface and aloft) few hours before and
 5 after the time of sunset (indicated with a black solid vertical line). Temporal variation of
 6 MBLM-derived (a) T , (b) r , (c) ΔT and (d) σ_{ws}^2 , sodar-derived (e) range-corrected SNR and (f)
 7 σ and profiler-derived (g) range-corrected SNR and (h) σ . The sodar- and profiler-derived
 8 parameters are plotted at 3 representative levels each (150, 300 and 450 m for sodar and 900,
 9 1500 and 2100 m for profiler). Vertical dashed lines indicate the start time of the transition as
 10 identified by different state variables.

11

12

13

14

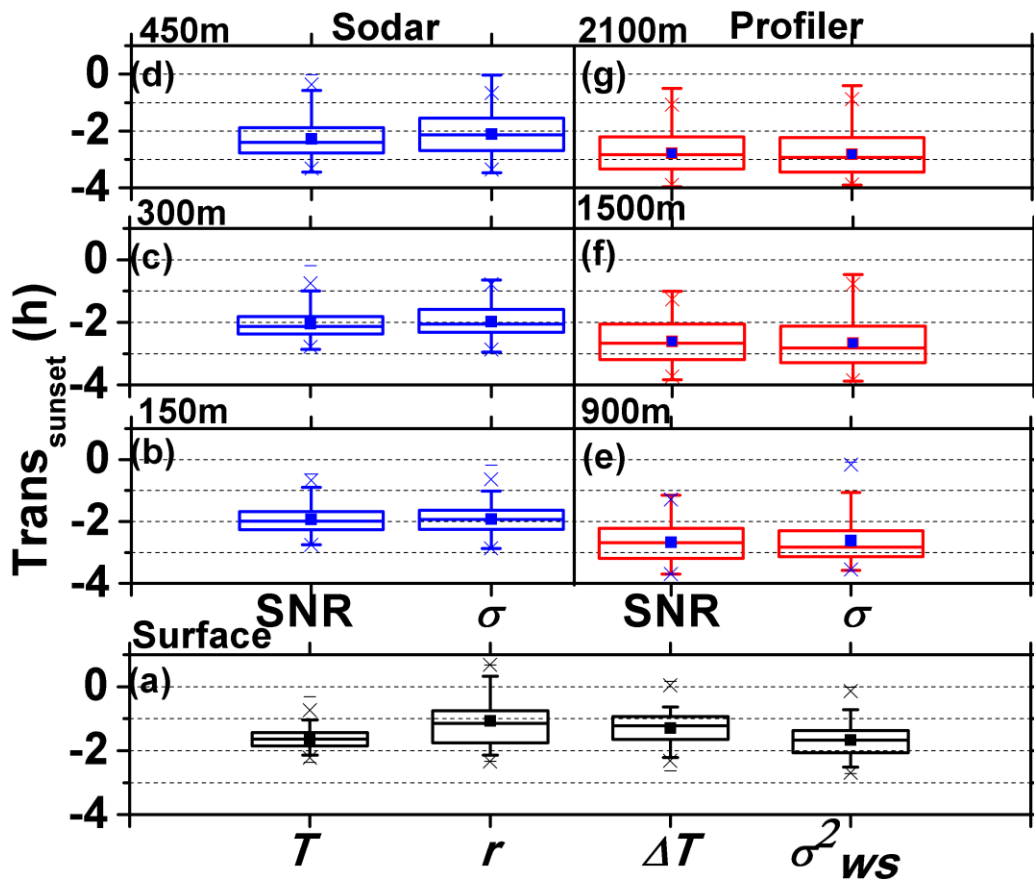
15

16

17

18

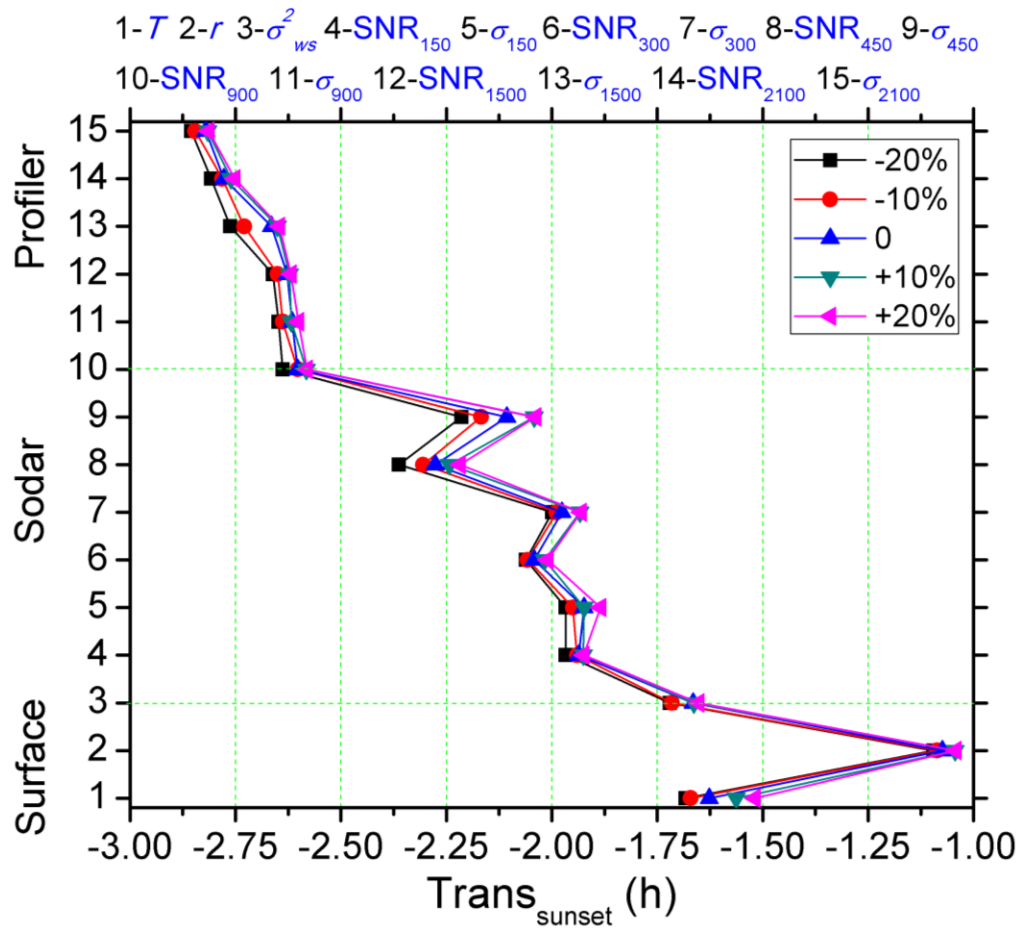
1
2
3



4
5
6
7
8
9
10
11
12
13
14
15
16
17
18
19
20
21

Figure 3: Distributions (in terms of box plot) of $\text{Trans}_{\text{sunset}}$ (= start time of AT - time of sunset) for different state variables, depicting the behaviour of transition start time with reference to the sunset time. Distributions for $\text{Trans}_{\text{sunset}}$ at (a) the surface (obtained from T , r , ΔT and σ_{WS}^2), (b)-(d) 150 m, 300 m and 450 m, respectively (obtained from sodar-derived range-corrected SNR and σ) and (e)-(g) 900 m, 1500 m and 2100 m, respectively (obtained from profiler-derived range-corrected SNR and σ).

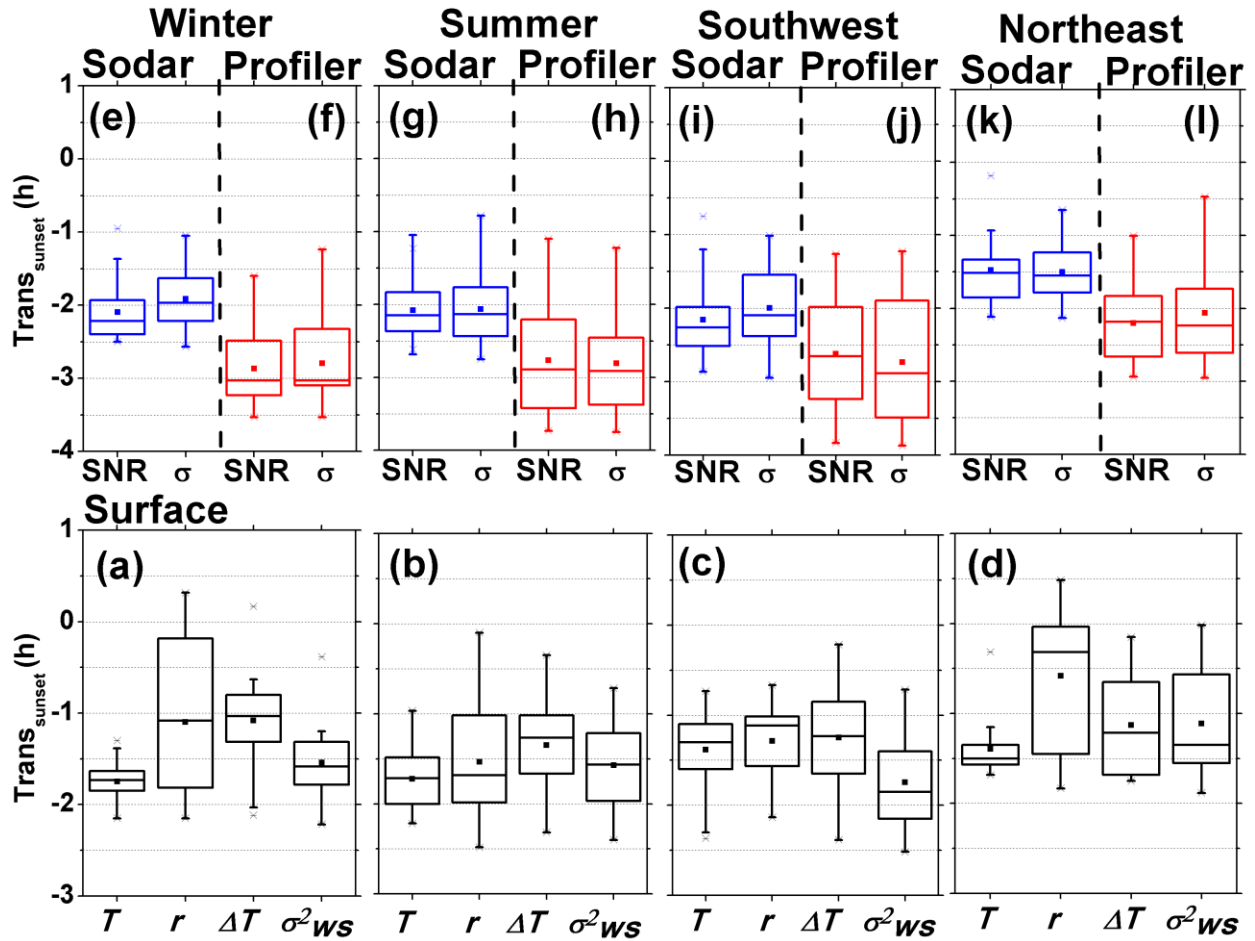
1
2



3
4 Figure 4: Vertical variation of mean $Trans_{sunset}$ as obtained by different state variables for
5 different thresholds, depicting the sensitivity of thresholds used in the present study on the start
6 time of transition.

7
8
9
10
11
12
13
14
15
16
17
18
19

1
2



3
4
5
6
7
8
9
10
11
12
13
14
15
16
17
18
19

Figure 5: The distributions of $Trans_{\text{sunset}}$ as obtained by different surface state variables for (a) winter (b) summer, (c) southwest monsoon and (d) northeast monsoon, depicting the seasonal variability in the start time of transition. The distributions for $Trans_{\text{sunset}}$ as obtained by sodar-derived range-corrected SNR and σ at 300 m for (e) winter, (g) summer, (i) southwest monsoon and (k) northeast monsoon, respectively. (f), (h), (j) and (l) are same as (e), (g), (i) and (k), except for profiler-derived range-corrected SNR and σ at 1500 m.

1
2
3
4
5
6
7
8
9
10
11
12
13
14
15
16
17
18
19
20
21
22
23
24
25

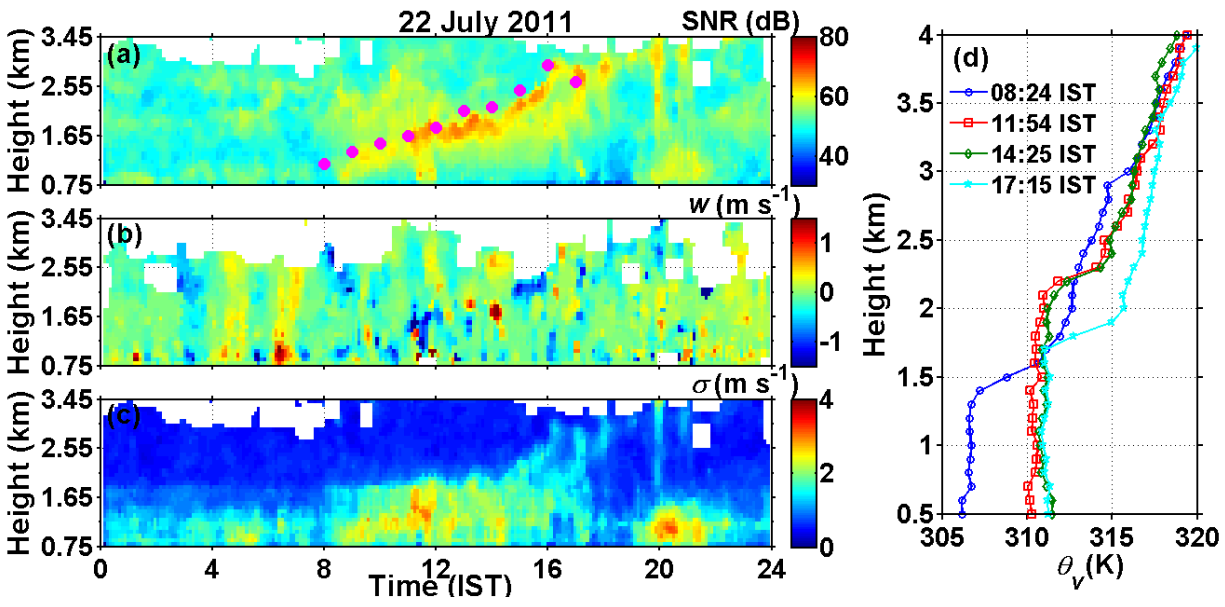
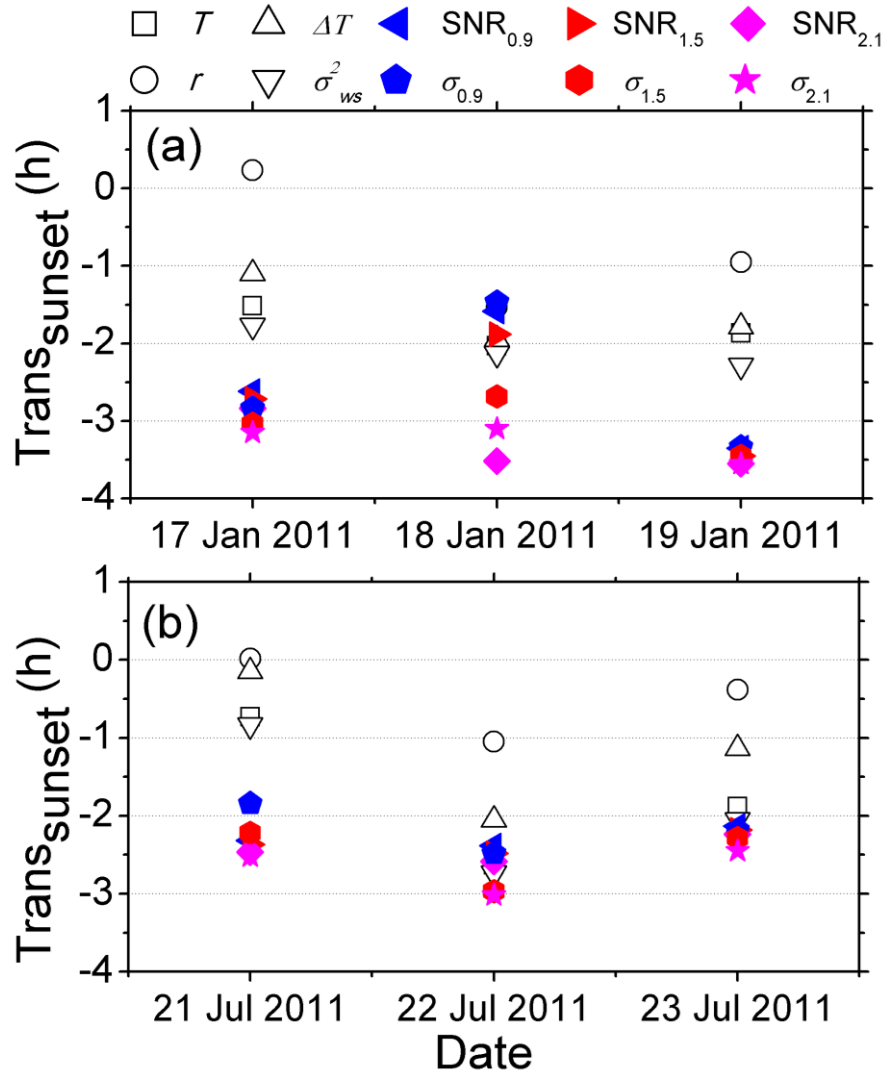


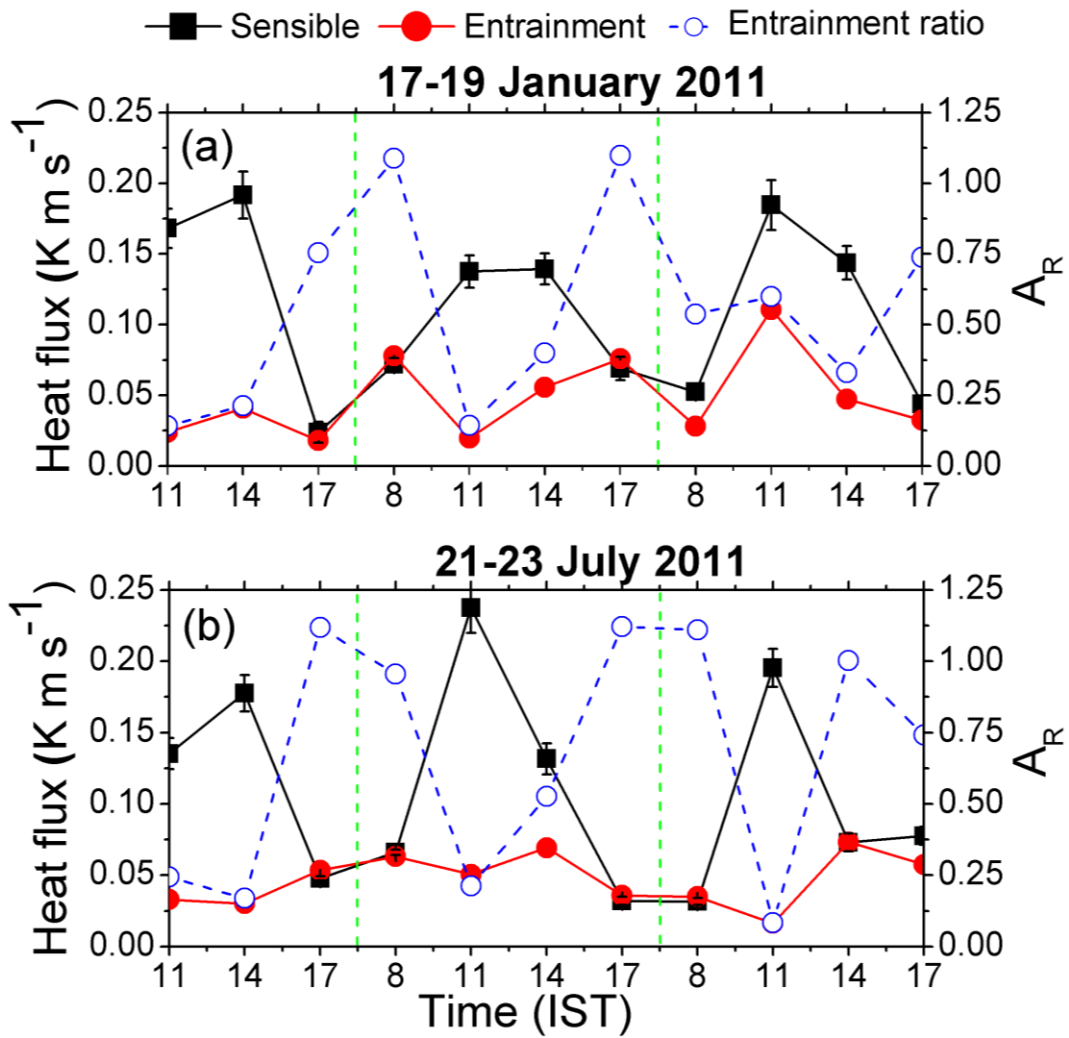
Figure 6: Diurnal variation of profiler attributes (a) range-corrected SNR (b) w and (c) σ on 22 July 2011, illustrating the evolution of ABL and afternoon transition. (d) The vertical variation of radiosonde-derived θ_v at ~ 3 h intervals. The solid symbols on (a) indicate the height of ABL.



1
2
3
4
5
6
7
8
9
10
11
12
13
14
15
16

Figure 7: The start time of AT with reference to the time of sunset as obtained by different state variables at the surface and aloft during (a) 17-19 January 2011 and (b) 21 - 23 July 2011.

1
2
3



4
5 Figure 8: Sensible and entrainment fluxes (left axis) and entrainment ratio (right axis) estimated
6 at ~ 3 h. intervals during (a) 17-19 January 2011 and (b) 21-23 July 2011, indicating the forcings
7 on ABL from the bottom and top.
8
9

